Iraqi Journal of Physics, 2026
https://doi.org/10.30723/ijp.v24i1.1427

Vol.24, No.1, PP. 1-11
P-ISSN: 2070-4003
E-ISSN: 2664-5548

Elastic and Inelastic Coulomb Transitions in ^{50,52}Cr

Mohammed M. Dhhewy[1*] and Arkan R. Ridha[1]
[1]*Department of Physics, College of Science, University of Baghdad, Baghdad, Iraq*
*Corresponding author: Mohammed.ma@sc.uobaghdad.edu.iq

Abstract

The elastic and inelastic longitudinal electron scattering form factors in of chromium isotopes (^{50,52}Cr) isotopes were studied using the radial wave functions of a transformed harmonic oscillator potential in the local scale transformation technique. Occupation numbers from configuration mixing using the Hsieh-Wildenthal (HW) method for ^{50,52}Cr were considered in parallel with those obtained using the adjusted occupation numbers. For shell interactions, the model space for HW interaction is restricted to the $1d_{3/2}$ and $1f_{7/2}$ subshells. The charge density distributions in the ground state and differential electron scattering cross-sections were computed. The inelastic form factors were studied by including core polarization using the Bohr-Mottelson model. For ^{50}Cr, the three C2 transitions and the two C4 transitions were investigated. For ^{52}Cr, the inelastic form factor for the two C2 transitions and for the two C4 transitions is investigated. In general, the use of the transformed harmonic-oscillator (THO) basis proved itself to be a good candidate to study stable nuclei, where good results (elastic and inelastic Coulomb form factors and differential cross sections) were obtained for ^{50,52}Cr isotopes.

Article Info.

Keywords:
Electron Scattering Differential Cross Section for ^{50,52}Cr, Charge Distributions, Charge rms Radii, Elastic and Inelastic Coulomb Form Factors, Energy Levels.

Article history:
Received: Jan. 30, 2025
Revised: May, 07, 2025
Accepted: May, 21, 2025
Published: Mar.01, 2026

1. Introduction

The computation of nuclear bulk quantities is of great importance in testing nuclear models and in understanding nuclear structure. One of these bulk quantities is those extracted from electron scattering off nuclei, such as rms charge radii, charge distributions, elastic and inelastic charge form factors and differential cross sections; i.e., the electromagnetic structure of nuclei which the probing to the nuclei is done through electromagnetic interaction [1-3]. Such interaction is relatively weak; therefore, it is experimentally reliable. The bulk quantities have been intensively relying on the used nuclear wave functions (WF) [4,5]. Such wave functions should be mainly characterized by Gaussian behavior at the central region and exponential behavior at large r [6]. Firstly, the harmonic-oscillator (HO) wave functions are analytically suitable, but with deficiency coming from the Gaussian fall-off behavior at large r [7]. The WFs of Woods-Saxon (WS) potential [8,9] were successfully used to investigate the ground and excited states in stable and unstable nuclei. Such potential was widely used but with a numerical solution to the radial Schrodinger equation. The pioneering approach to solving the radial Schrodinger for WS potential is using Nikiforov–Uvarov Tanique [10]. Besides, the transformed harmonic-oscillator (THO) WFs were largely employed to study the properties of stable and exotic nuclei [11]. The results using THO WFs were very good and promising, in agreement with empirical data. Such WFs basis improves the performance of HO WFs at large r to be exponential while it leaves the central Gaussian part intact. Another approach is to use the WFs of the mean-field in Hartree-Fock (HF) with Skyrme forces [12-14]. Fluctuating results mainly characterize such an approach. The Cosh potential is another good option to be used to study stable and exotic nuclei [15,16]. The Ginocchio potential was rarely used to investigate the bulk properties of nuclei [17]. Unfortunately, such potential is cumbersome due to the existence of more than three parameters to regenerate the experimental size radii and single-nucleon binding energies. The spherical Bessel and Hankel functions have been successfully used for both stable exotic nuclei [18,19]. The Hulthen potential [20] for asymptotic limit has been used with very good success to study some light nuclei.

In the present work, we undertook the study of ground and excited states of Chromium isotopes (^{50,52}Cr). Such isotopes were previously studied experimentally as in the refs. [21,22]. Our theoretical calculations were based on using the WFs of THO in the local scaling transformation (LST) technique, which was not used before on such isotopes. Due to the large model space of fp-shell which leads to cumbersome calculations, the Hsieh-Wildenthal (HW) interaction [23] was used for ^{50,52}Cr isotopes. The model space for HW interaction is $1d_{3/2}$ and $1f_{7/2}$ for HW interaction. Such interaction was a good candidate to initiate the elastic and inelastic calculations for the studied aforementioned ^{50,52}Cr. The inelastic Coulomb form factors were calculated by the inclusion of core-polarization (CP) using Bohr-Mottelson (B-M), Tassie (T), and valence (V) models.

2. Theory

The radial WFs of THO in the formulation of LST are given by [24]:

$$R^{THO}_{nlj,n/p}(r) = \frac{f(r,\gamma_{n/p},m)}{r}\sqrt{\frac{df(r,\gamma_{n/p},m)}{dr}}\,R_{nl}\big(f(r,\gamma_{n/p},m),b_{n/p}\big) \qquad \mathbf{(1)}$$

where n, l, and j are the principle, orbital, and total spin quantum numbers. The n/prepresents the neutron/proton. The $b_{n/p}$, stands for the HO size parameter for neutrons/protons. In Eq. (1), $f(r,\gamma_{n/p},m)$ denotes the scale function given by [24]:

$$f(r,\gamma_{n/p},m) = \left(\frac{1}{\left(\frac{1}{r}\right)^m + \left(\frac{1}{\gamma\sqrt{r}}\right)^m}\right)^{\frac{1}{m}} \qquad \mathbf{(2)}$$

The derivative to scale function can be written as:

$$\frac{df(r,\gamma_{n/p},m)}{dr} = \frac{-\left(\frac{1}{\left(\frac{1}{r}\right)^m + \left(\frac{1}{\gamma\sqrt{r}}\right)^m}\right)^{\frac{1}{m}}\left(-\frac{m\left(\frac{1}{r}\right)^m}{r} - \frac{m\left(\frac{1}{\gamma\sqrt{r}}\right)^m}{2r}\right)}{m\left(\left(\frac{1}{r}\right)^m + \left(\frac{1}{\gamma\sqrt{r}}\right)^m\right)} \qquad \mathbf{(3)}$$

In Eqs. (1) to (3), the m and $\gamma_{n/p}$ represent an integer and real constants controlling the shape of the wave function at the asymptotic region.

The density distribution for n/p in pure configuration for any nuclear sample is given by [8]:

$$\rho_{n/p}(r) = \frac{1}{4\pi}\sum_{nlj} \mathbb{O}_{nlj,n/p}\left|R^{THO}_{nlj}(r,b_{n/p})\right|^2 \qquad \mathbf{(4)}$$

The $\mathbb{O}_{nlj,n/p}$, represents the occupation numbers. In mixing configuration, the density is given by [7]:

$$\rho_{CJ,n/p}(r) = \frac{1}{\sqrt{4\pi}} \frac{1}{\sqrt{2J_i + 1}} \sum_{ab} \mathcal{X}^{J_f\ J_i\ J}_{a,b,n/p} \langle j_a \| Y_J \| j_b \rangle R^{THO}_{n_a l_a j_a,n/p}(r) R^{THO}_{n_b l_b j_b,n/p}(r) \tag{5}$$

The $\mathcal{X}^{J_f\ J_i\ J}_{a,b,n/p}$ in the above equation denotes the weight of transition [25], evaluated from Nushell shell model code [26]. In addition, a and b stands for the quantum numbers of individual nucleons in the final and initial states, respectively.

Eventually, the charge density is evaluated from the folding procedure for the density of protons and neutrons followed in ref. [27], i.e.,

$$\rho_{ch}(r) = \rho_{ch,n}(r) + \rho_{ch,p}(r) \tag{6}$$

where $\rho_{ch,n}(r)$ and $\rho_{ch,p}(r)$ indicates the total charge distributions for all neutrons and protons, correspondingly.

The size radii for nuclei under study are computed from [27]:

$$\langle r^2 \rangle_i^{\frac{1}{2}} = \sqrt{\frac{4\pi}{i} \int_0^{\infty} \rho_i(r) r^4 dr} \tag{7}$$

where i in the above equation denotes the number of neutrons $(i \equiv N)$ or protons $(i \equiv Z)$ or nucleons $(i \equiv A)$ or $(i \equiv ch = Z)$.

The longitudinal form structures for electron scattering in the Born approximation for the first-order is given by [25, 28-29]:

$$F^C_{J,ch}(q) = \frac{1}{Z} \sqrt{\frac{4\pi}{(2J_i + 1)}} \sum_{\frac{n}{p}} \langle J_f \left\| \boldsymbol{O}^C_J \left(q, \frac{n}{p}\right) \right\| J_i \rangle f_{\frac{n}{p}}(q) \tag{8}$$

The $f_{n/p}(q)$ represents the charge form factor for single proton or neutron [27]. The longitudinal transition operator in Eq. (8) is given by [25]:

$$\boldsymbol{O}^C_{JM_J}(q, n/p) = \int j_J(qr)\, Y_{JM_J}(\Omega_r) \hat{\rho}_{n/p}(\vec{r}) d\vec{r} \tag{9}$$

The details of spherical Bessel function $(j_J(qr))$, density operator $(\hat{\rho}_{n/p}(\vec{r}))$ and spherical harmonics $(Y_{JM_J}(\Omega_r))$ can be found in ref. [30].

In Eq. (8), the many-nucleon matrix element is related to the individual nucleon matrix element by [25]:

$$\langle J_f \| \boldsymbol{O}^C_J(q, n/p) \| J_i \rangle = \sum_{ab} X^{J_i,J_f,J}_{a,b,p/n} \langle b, n/p \| O^C_J(q, r, t_z) \| a, n/p \rangle \tag{10}$$

The charge form factors for any multipolarity (J) can be accounted for from

$$F_{J,ch}(q) = \frac{4\pi}{Z}\int_{0}^{\infty} j_J(qr)\rho_{J,ch}(r)r^2 dr \tag{11}$$

The transition charge density ($\rho_{J,ch}(r)$), in Eq. (11) is divided into two parts, one for the core polarization (CP) and the other for model space [25], i.e.,

$$\rho_{ch,J}(r) = \rho_{ch,J}^{CP}(r) + \rho_{ch,J}^{MS}(r) \tag{12}$$

The $\rho_{ch,J}^{CP}(r)$ in Eq. (12), is evaluated using T [31,32], B-M [33] and valence [25] models as follows:

$$\rho_{ch,J}^{CP,T}(r) = N_T r^{J-1}\frac{d}{dr}\rho_{ch}(r) \tag{13}$$

$$\rho_{ch,J}^{CP,B-M}(r) = N_{B-M}\frac{d}{dr}\rho_{ch}(r) \tag{14}$$

and

$$\rho_{ch,J}^{CP,V}(r) = N_V \rho_{ch}(r) \tag{15}$$

The N in Eqs. (13), (14) and (15) are accounted to produce the experimental quadrupole moments. Finally, the $\rho_{J,ch}^{MS}(r)$ in Eq. (12) is evaluated from the active nucleons in the selected model space, as follows [7]:

$$\rho_{CJ,n/p}(r) = \frac{1}{\sqrt{4\pi}}\frac{1}{\sqrt{2J_i+1}}\sum_{ab} X_{a,b,n/p}^{J_f\ J_i\ J}\left\langle j_a\middle\|Y_J\middle\|j_b\right\rangle R_{n_a l_a j_a,\frac{n}{p}}(r)R_{n_b l_b j_b,\frac{n}{p}}(r) \tag{16}$$

3. Results and Discussion

With the adoption of the nuclear shell model, a cumbersome huge model space is encountered especially for fp-shell nuclei. Therefore, a reduction in the model space is required. As a result of that, the HW interaction [23] was adopted for ^{50,52}Cr with ${}^{32}_{16}S_{16}$ as a core. The model spaces for HW interaction are $1d_{3/2}1f_{7/2}$ subshells. The run of the nuclear shell model Nushell [26] is used to obtain the $X_{a,b,n/p}^{J_f\ J_i\ J}$. The Nushell code uses HO, WS and HF WFs, besides, many empirical effective interactions were included in the library in Nushell code. In parallel with the shell calculations, the wave functions of modified HO WFs are used instead of the HO basis.

For the theoretical calculations, firstly, the elastic charge densities, form factors, and differential cross sections are studied. Two occupation numbers were used; the first is the adjusted occupation numbers adopted to generate the available empirical size charge radii (see Table 1). The second is the occupation numbers obtained from configuration mixing by running the Nushell shell model code (see Table 2). The spin and isospin quantum numbers, parity, and parameters of modified HO WFs are presented in Table 3. The b_p, m and γ_p were fixed so as to produce the experimental rms charge radii [21]. For the fixed parameters of calculations presented in Table 1, the calculated charge size radii are presented in Table 4.

In Fig. 1, the computed charge densities are displayed by dashed and solid curves for adjusted and interactional occupation numbers, respectively. The dotted symbols represent empirical data taken from [21]. It is found that the results of adjusted occupation numbers are in very good match with empirical data for ^{52}Cr while there is a slight overestimation in the calculation for ^{50}Cr.

In Fig. 2, the elastic form structures for ^{50,52}Cr are portrayed by solid and dashed curves for adjusted and interactional occupation numbers, respectively. The dotted symbols represent empirical data taken from [22]. It was also found that the results of adjusted occupancies were in good match with empirical data.

The computed differential cross sections were drawn in Fig. 3 for ^{50,52}Cr. The calculations were based on using adjusted occupancy numbers only. The dashed, dashed-doted, and solid curves represent the calculated differential cross sections with incident energies of 200, 398.2, and 401.6 MeV, respectively. The empirical data are presented by triangle symbol 200 MeV, plus symbol 398.2 MeV and dotted symbol 401.6 MeV. The results are in very good match with the experimental data.

In Table 5, the calculated excitation energy using Nushell code were presented and compared with experimental values. It is seen that the predicted values using HW interaction for ^{50,52}Cr are remarkably good in comparison with experimental values. The calculated values are ascribed to the HW interaction, such empirical interaction is in the Nushell library.

For inelastic Coulomb form factors, the theoretically studied Coulomb transitions were depicted in Figs. 4 and 5 for ^{50,52}Cr, respectively. The calculations took into account the contribution of core-polarization (CP). The CP in the present work, was calculated from three macroscopic models; B-M, T, and V models. The short dashed, long dashed, and solid curves stand for the V, B-M, and T, correspondingly.

Figs. 4 (a), (b), (c), (d) and (e) for ^{50}Cr represent the transitions: $0^+ \rightarrow 2^+_1$ $(E_x = 0.78\,MeV)$, $0^+ \rightarrow 2^+_2$ $(E_x = 2.92\,MeV)$, $0^+ \rightarrow 2^+_3$ $(E_x = 3.16\,MeV)$, $0^+ \rightarrow 4^+_1$ $(E_x = 1.88\,MeV)$ and $0^+ \rightarrow 4^+_{2,}$ $(E_x = 3.32\,MeV)$, respectively. From the plotted results, it is noted in Figs. 4 (c) and (d) for the transition $0^+ \rightarrow 2^+_3$ $(E_x = 3.16\,MeV)$ and $0^+ \rightarrow 4^+_1$ $(E_x = 1.88\,MeV)$ which the results of the B-M, T, and V models are in poor agreement with experimental data, unlike the other transitions which are well explained by B-M model.

The Figs. 5 (a), (b), (c) and (d) for ^{52}Cr represent the transitions: $0^+ \rightarrow 2^+_1$ $(E_x = 1.43\,MeV)$, $0^+ \rightarrow 2^+_4$ $(E_x = 3.77MeV)$, $0^+ \rightarrow 4^+_1(E_x = 2.37\,MeV)$ and $0^+ \rightarrow 4^+_2$ $(E_x = 2.77\,MeV)$, respectively. It is noted in Fig. 5(b) for the transition $0^+ \rightarrow 2^+_4$ $(E_x = 3.77MeV)$ which the Bohr-Mottelson, Tassie and valence models failed in to explain the experimental data contrary to the other transitions which are well explained by the B-M model.

In general, it is found that the results of B-M are better than the results of T and V models. The results of the V model were found in a poor match with empirical data for all studied transitions.

It is worth mentioning that with the dominance of small deformation, the B-M model elucidates the laboratory data, unlike the T model which succeeds in nuclei with large deformation. The ^{50,52}Cr nuclei are even-even nuclear samples, therefore, one expects small deformations due to the high stability of such nuclei. The failure of the results of valence model is due to its simple form representation for deformation (see Eq. (15)).

Table 1: Calculated proton occupation numbers ($\mathbb{O}_{nlj,p}$) from Nushell for $^{50}_{24}Cr_{26}$ and $^{52}_{24}Cr_{28}$ nuclei.

nl$_j$	$^{50}_{24}Cr_{26}$	$^{52}_{24}Cr_{28}$
$1s_{1/2}$	2.0	2.0
$1p_{3/2}$	4.0	4.0
$1p_{1/2}$	2.0	2.0
$1d_{5/2}$	6.0	6.0
$1d_{3/2}$	3.806	3.766
$2s_{1/2}$	2	2
$1f_{7/2}$	4.194	4.234

Table 2: Adjusted proton occupation numbers ($\mathbb{O}_{nlj,p}$) from Nushell for $^{50}_{24}Cr_{26}$ and $^{52}_{24}Cr_{28}$ nuclei.

$\mathbf{nl}_j$	$^{50}_{24}Cr_{26}$	$^{52}_{24}Cr_{28}$
$1s_{1/2}$	2.0	1.9
$1p_{3/2}$	4.0	4.0
$1p_{1/2}$	2.0	2.0
$1d_{5/2}$	6.0	6.0
$1d_{3/2}$	4.0	4.0
$2s_{1/2}$	1.4	1.2
$1f_{7/2}$	2.8	4.9
$1f_{5/2}$	1.4	-
$2p_{1/2}$	0.4	-

Table 3: Total spin, isospin, and the parameters of THO.

$^{A}_{Z}X_N$	$J^{\pi}T$	b_p	m	γ_p
$^{50}_{24}Cr_{26}$	$0^{+}1$	2.000	8	1.737
$^{52}_{24}Cr_{28}$	$0^{+}2$	1.990	10	2.182

Table 4: Evaluated rms proton and charge radii for $^{50}_{24}Cr_{26}$ and $^{52}_{24}Cr_{28}$ nuclei.

$^{A}_{Z}X_N$	*Calculated* $\langle r_p^2\rangle^{1/2}$	*Calculated* $\langle r_{ch}^2\rangle^{1/2}$	*Exp.* $\langle r_{ch}^2\rangle^{1/2}$ *[21]*
$^{50}_{24}Cr_{26}$	2.457	3.707	3.707(15)
$^{52}_{24}Cr_{28}$	2.288	3.684	3.684(15)

Table 5: Calculated and experimental excitation energies Ex (in MeV) for selected transitions in 50Cr and 52Cr. The transitions are from the 0+ ground state to excited 2+ and 4+ states. Theoretical results are compared with empirical data from [22].

Isotope	$J_i^{+}T \rightarrow J_f^{+}T$	**Calculated** $E_x(MeV)$	**Empirical[22]** $E_x(MeV)$
$^{50}_{24}Cr_{26}$	$0^{+} \rightarrow 2_1^{+}$	0.882	0.78
	$0^{+} \rightarrow 2_2^{+}$	2.803	2.92
	$0^{+} \rightarrow 2_3^{+}$	3.505	3.16
	$0^{+} \rightarrow 4_1^{+}$	1.895	1.88
	$0^{+} \rightarrow 4_{2,}^{+}$	3.012	3.32
$^{52}_{24}Cr_{28}$	$0^{+} \rightarrow 2_1^{+}$	1.183	1.43
	$0^{+} \rightarrow 2_4^{+}$	7.100	3.77
	$0^{+} \rightarrow 4_1^{+}$	2.046	2.37
	$0^{+} \rightarrow 4_2^{+}$	2.538	2.77

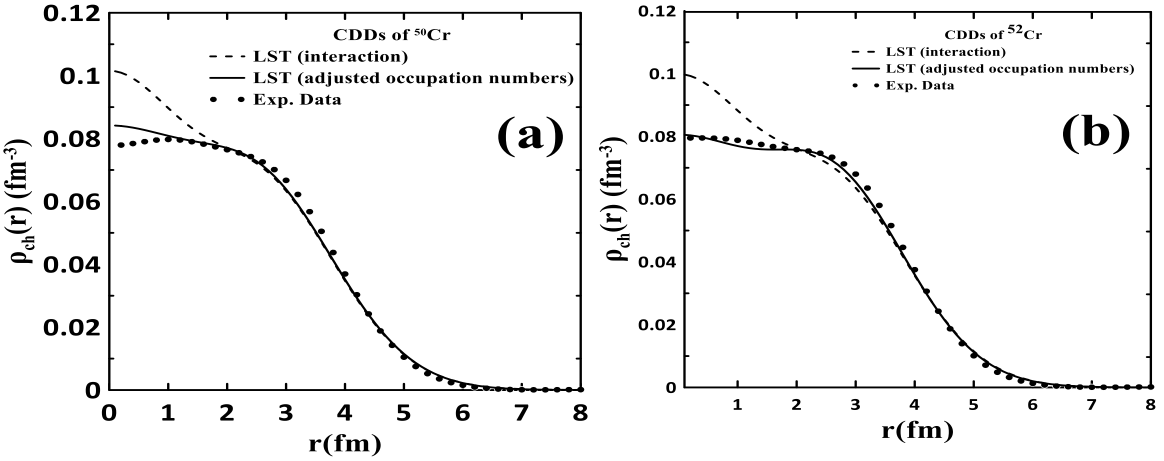

Figure 1: Computed and experimental charge density distributions (CDDs) for ^{50} Cr (a) and ^{52}Cr (b). Dashed curves use shell-model occupancies, solid curves use adjusted values, and filled symbols represent experimental data from [21].

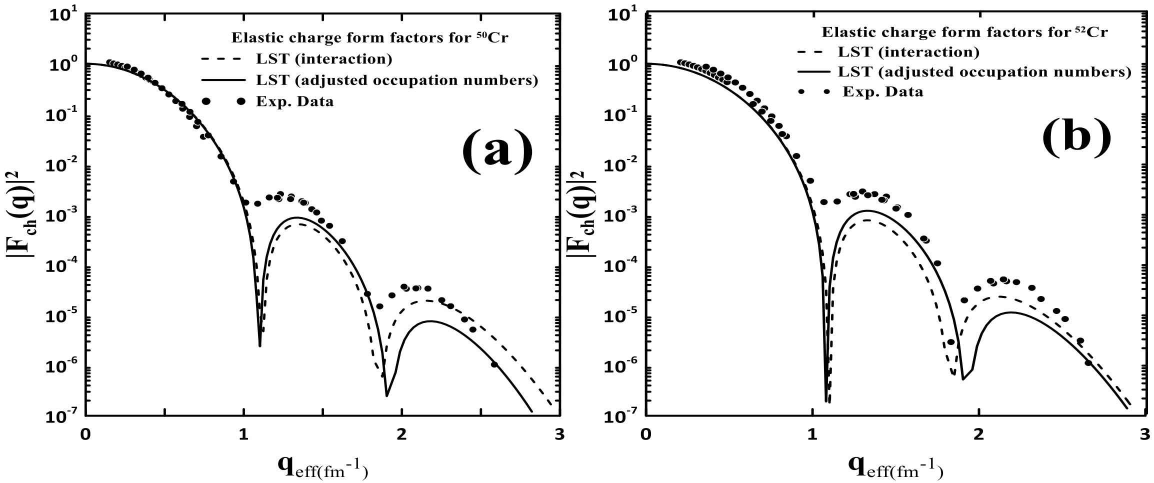

Figure 2: Elastic charge form factors for ^{50}Cr (a) and ^{52}Cr (b). Dashed and solid curves represent theoretical predictions using shell-model and adjusted occupation numbers, respectively. Experimental data points are shown as filled symbols [22].

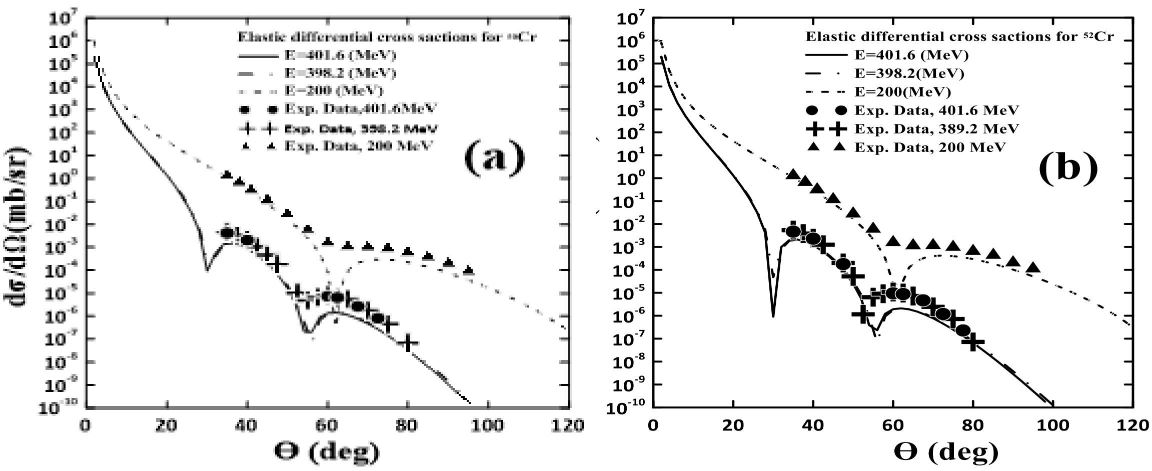

Figure 3: Computed and experimental differential cross-sections $\left(\frac{d\sigma}{d\Omega}\right)$ *for ^{50,52}Cr were portrayed for incident electron energies of 200 MeV, 398.2 MeV, and 401.6 MeV represented by short-dashed, dashed, dotted, and solid carve, respectively. The empirical data are represented by a triangle, plus and dotted symbols [22].*

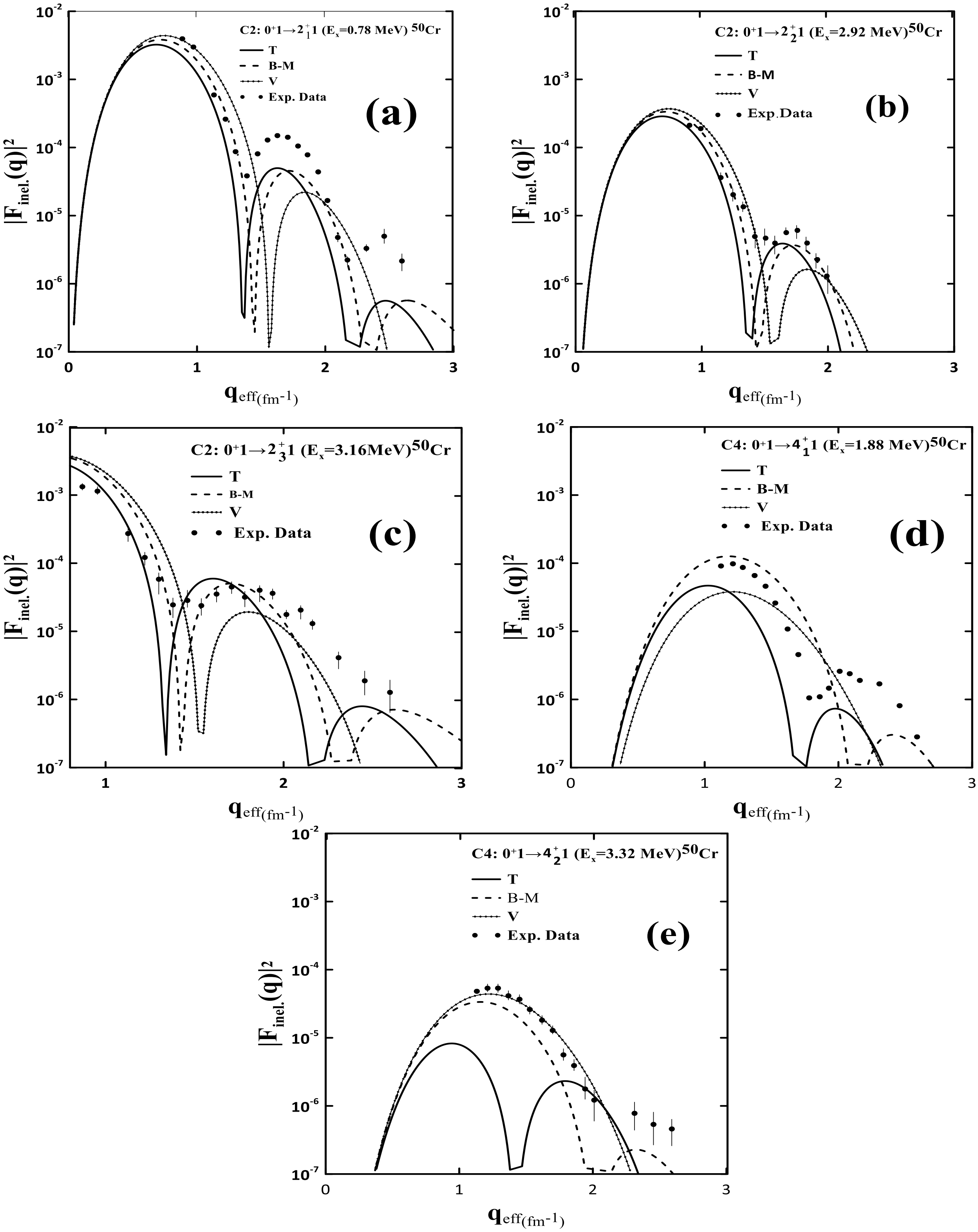

Figure 4: Inelastic transitions related to the C2 and C4 form factors of ^{50}Cr for the $2_1^+(a)$, $2_1^+(b)$, $2_3^+(c)$, $4_1^+(d)$ and $4_2^+(e)$. The theoretical results were computed using Tassie, Bohr-Mottelson, and valence models represented by solid, dashed and solid diamond curves. The empirical data were represented by filled dotted symbols [22].

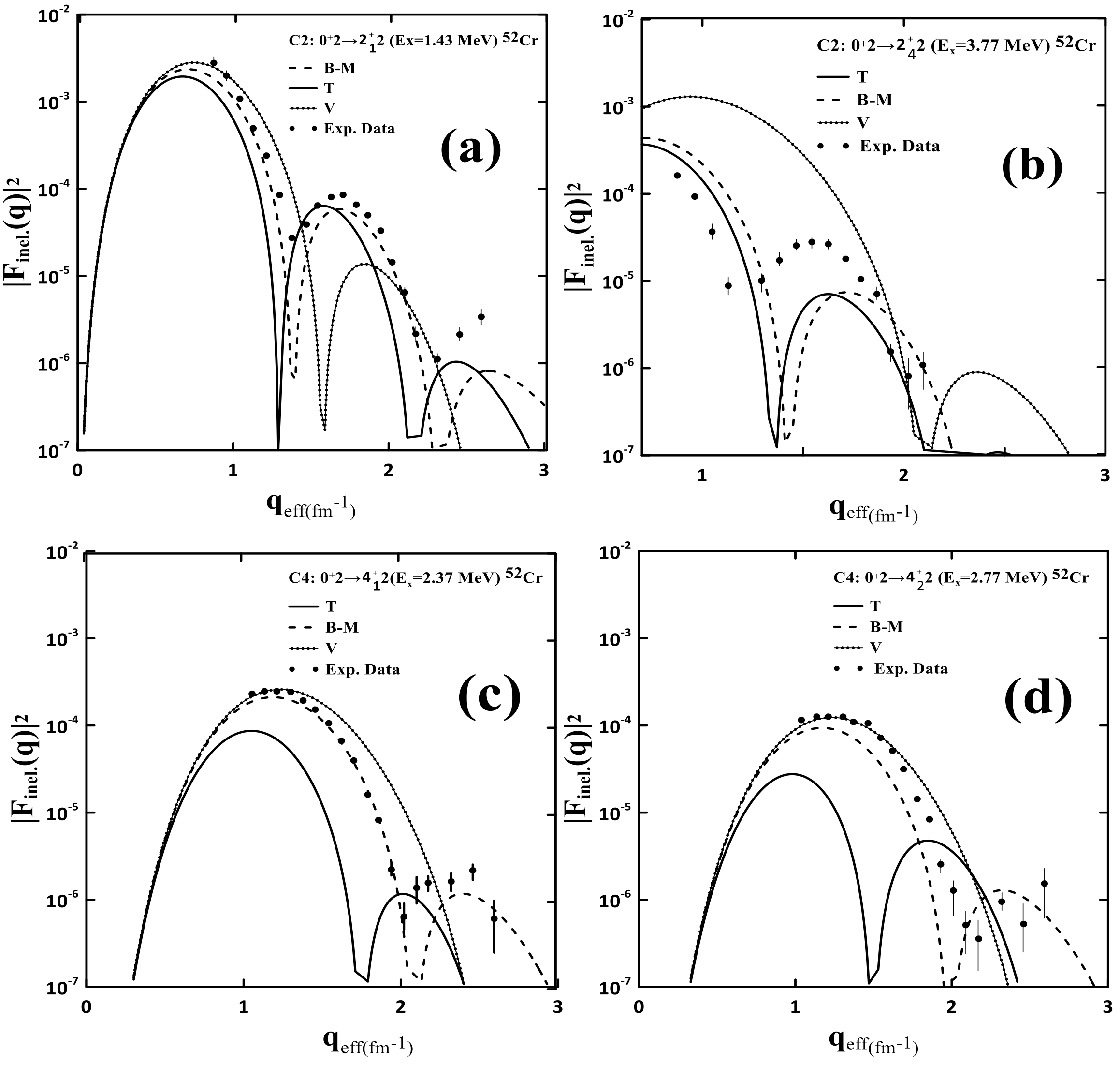

Figure 5: Inelastic transitions related to the C2 and C4 form factors of ^{52}Cr for $2^+_1(a)$, $2^+_4(b)$, $4^+_1(c)$ and $4^+_2(d)$. The theoretical results were computed using Tassie, Bohr-Mottelson, and valence models represented by solid, dashed and solid-diamonds curves. The empirical data were represented by filled dotted symbols [22].

4. Conclusions

In summary, using modified oscillator wave functions greatly enhanced the results for the charge densities and both elastic and inelastic longitudinal form factors of ^{50,52}Cr when compared to real-world data. The model spaces for empirical HW effective interaction were used to investigate the isotopes ^{50,52}Cr. The HW interaction was used with (16^32)S_16 (core) plus 18 and 20 nucleons (in the model space) for ^{50}Cr and ^{52}Cr, respectively. The results of the calculated elastic electron scattering differential cross section were found in excellent agreement with experimental ones. In general, the computed energy levels for ^{50,52}Cr were found to be in very good agreement with experimental data for HW interaction. For the computed inelastic Coulomb form factors, the core polarization was accounted for using macroscopic Bohr-Mottelson, Tassie, and valence models. Overall, the theoretical results showed that the Bohr-Mottelson model matched the experimental data better than the Tassie and valence models. The three CP models failed only in explaining the transitions: 0^+→2_3^+ (E_x= 3.16 MeV) and 0^+→4_1^+ (E_x=1.88 MeV) in ^{50}Cr, 0^+→2_4^+ (E_x=3.77MeV) in ^{52}Cr. The computed results of the valence model were in poor match with those of empirical data. The Bohr-Mottelson and valence models apply to nuclei with small deformations, whereas the Tassie model is more successful in nuclei with large deformations. The poor agreement of the results of the valence model is attributed to its simple mathematical form.

Conflict of interest

The authors declare that they have no conflict of interest.

References

1. C. J. Batty, E. Friedman, H. J. Gils, and H. Rebel, Adv. Nucl. Phy. **19**, 1 (1989). https://doi.org/10.1007/978-1-4613-9907-10_1.
2. A. A. M. Hussein and G. N. Flaiyh, East Eur. J. Phys. **2023**, 82 (2023). https://doi.org/10.26565/2312-4334-2023-1-09.
3. G. N. Flaiyh and S. A. Rahia, Iraqi J. Phys. **19**, 60 (2021). https://doi.org/10.30723/ijp.v19i50.675.
4. A. N. Antonov, P. E. Hodgson, and I. Z. Petkov, Nucleon Momentum and Density Distributions in Nuclei (Clarendon Press. UK, 1988).
5. D. Murshedi and A. D. Salman, J. Nucl. Sci. **7**, 1 (2021). https://doi.org/10.1501/nuclear.2023.50.
6. C. A. Bertulani, Nuclear Physics in a Nutshell (Princeton University Press, 2007). https://doi.org/10.1515/9781400839322.
7. A. R. Radhi, A. K. Hamoudi, and A. R. Ridha, Iraqi J. Sci. **54**, 324 (2013).
8. S. Gamba, G. Ricco, and G. Rottigni, Nuclear Physics A, **213**, 383(1973). https://doi.org/10.1016/0375-9474(73)90159-0.
9. A. R. Ridha and W. Z. Majeed, Iraqi J. Sci. **63**, 977 (2022). https://doi.org/10.24996/ijs.2022.63.3.7.
10. E. Yazdankish, Int. J. Mod. Phys. E, **29**, 2050032 (2020). https://doi.org/10.1142/S0218301320500329.
11. H. F. Ojaimi and A. R. Ridha, in 2022 International Congress on Human-Computer Interaction, Optimization and Robotic Applications (HORA), IEEE, 1 (2022). https://doi.org/10.1109/HORA55278.2022.9799913.
12. A. Fatah and A. Mohammed, Kirkuk Univ. Journal-Scientific Stud., **18**, 15 (2023). https://doi.org/10.32894/kujss.2023.138864.1096.
13. A. A. Alzubadi and L. J. Abbas, Phys. At. Nucl. **86**, 370 (2023). https://doi.org/10.1134/S1063778823040026.
14. O. Q. Afar and F. Z. Majeed, J. Phys. Conference Series, **1829**, 012026 (2021). https://doi.org/10.1088/1742-6596/1829/1/012026.
15. M. E. Grypeos, G. A. Lalazissis, S. E. Massen, and C. P. Panos, Journal of Physics G: Nuclear and Particle Physics, **17**, 1093 (1991), https://doi.org/10.1088/0954-3899/17/7/008.
16. S. S. Odah and A. R. Ridha,in AIP Conf. Proc. **2437**, 020115 (2022). https://doi.org/10.1063/5.0092614.
17. J. N. Ginocchio, Ann. Phys. (N. Y). **159**, 467 (1985). https://doi.org/10.1016/0003-4916(85)90120-4.
18. S. A. J. Khalaf and A. R. Ridha, Iraqi J. Sci. **64**, 668 (2023). https://doi.org/10.24996/ijs.2023.6.
19. S. A. J. Khalaf and A. R. Ridha, in AIP Conf. Proc. AIP Publishing, **2922**, 090005 (2024). https://doi.org/10.1063/5.0183082.
20. A A. Laid, J. A. Tostevin, and R. C. Johnson, Physical Review C, **48**, 1307 (1993). https://doi.org/10.1103/PhysRevC.48.1307.
21. H. De Vries, C. W. De Jager, and C. De Vries, At. Data Nucl. Data Tables, **36**, 495 (1987). https://doi.org/10.1016/0092-640X(87)90013-1.
22. J. W. Lightbody, Jr. J. B.Bellicard, J. M. Cavedon, B.Frois, D. Goutte, M. Huet, Ph. Leconte, A. Nakada, Phan Xuan Ho, S. K. Platchkov, and S. Turck-Chieze, Phys. Rev. C **27**, 113 (1983). https://doi.org/10.1103/PhysRevC.27.113.
23. S. T. Hsieh, X. Ji, R. Mooy, and B. H. Wildenthal, in AIP Conf. Proc. **142**, 357 (1986). https://doi.org/10.1063/1.35637.
24. S. Karataglidis and K. Amos, Phys. Rev. C, **71**, 064601 (2005). https://doi.org/10.1103/PhysRevC.71.064601.
25. B.A. Brown, B.H. Wildenthal, C. F. Williamson, F. N. Rad, and S. Kowalski, Phys. Rev. C, **32**, 1127 (1985). https://doi.org/10.1103/PhysRevC.32.1127.
26. B. A. Brown and W. D. M. Rae, "Nushell @ MSU, MSU-NSCL report" 1 (2007).
27. L. R. B. Elton, Nuclear Sizes. (Oxford University Press, 1961).
28. T. de Forest and J. D. Walecka, Adv. Phys. **15**, 1 (1966). https://doi.org/10.1080/00018736600101254.
29. Falah H. Abd and Mohanad H. Oleiwi, in AIP Conf. Proc. **2398**, 020032 (2022). https://doi.org/10.1063/5.0093637.

30. G. B. Arfken, H. J. Weber, and F. E. Harris, Mathematical Methods for Physicists (Elsevier, 2013). https://doi.org/10.1016/C2009-0-30629-7.
31. A. N. Bohr and B. R. Mottelson, Nuclear Structure (World Scientific, 1998).
32. M. H. Oleiwi, Science and Technology of Nuclear Installations **2021**, 020032 (2021). https://doi.org/10.1155/2021/6639185.
33. J. A. M. W. Greiner, Nuclear Models (Springer-Verlag Berlin Heidelberg New York, 1996). https://doi.org/10.11107/978·3·642·609711·1.

الانتقالات الكولومية المرنة وغير المرنة في ^{50,52}Cr

محمد محمود ضحيوي[1] وأركان رفعه رضا[1]
[1] قسم الفيزياء، كلية العلوم، جامعة بغداد، العراق

الخلاصة

تمت دراسة عوامل شكل التشتت الإلكتروني الطولي المرن وغير المرن في نظائر الكروم التوافقي المحول في تقنية تحويل المقياس المحلي. تم اعتبار أرقام الإشغال من خلط التكوين باستخدام طريقة هسيه-ويلدنثال (HW) لـ ^{50,52}C بالتوازي باستخدام الدوال الموجية الشعاعية ($^{50،52}$Cr) لجهد المذبذب مع تلك التي تم الحصول عليها باستخدام أرقام الإشغال المعدلة. بالنسبة لتفاعلات الغلاف، يقتصر الفضاء النموذجي لتفاعل HW على الغلافات الفرعية 1 $d_{3/2}$و $1f_{7/2}$. تم حساب توزيعات كثافة الشحنة في الحالة الأرضية والمقاطع العرضية للتشتت الإلكتروني التفاضلي. تمت دراسة عوامل الشكل غير المرنة من خلال تضمين استقطاب القلب باستخدام نموذج بور-موتلسون. بالنسبة لـ ^{50}Cr، تم التحقيق في انتقالات C2 الثلاثة وانتقاليC4 بالنسبة لـ ^{52}Cr، تم التحقيق في عامل الشكل غير المرن لانتقالي C2 ولانتقالي C4 بشكل عام، أثبت استخدام أساس المذبذب التوافقي المحول (THO) أنه مرشح جيد لدراسة النوى المستقرة، حيث تم الحصول على نتائج جيدة (عوامل الشكل الكولومبي المرنة وغير المرنة والمقاطع العرضية التفاضلية) لنظائر $^{50،52}$Cr.

الكلمات المفتاحية: توزيع الشحنة، المقطع العرضي التفاضلي للاستطارة الالكترونية المرنة، عامل التشكل الكولومي للاستطارة المرنة وغير المرنة، مربع نصف قطر الشحنة، مستويات الطاقة.